Journal of Materials Chemistry A

Accepted Manuscript

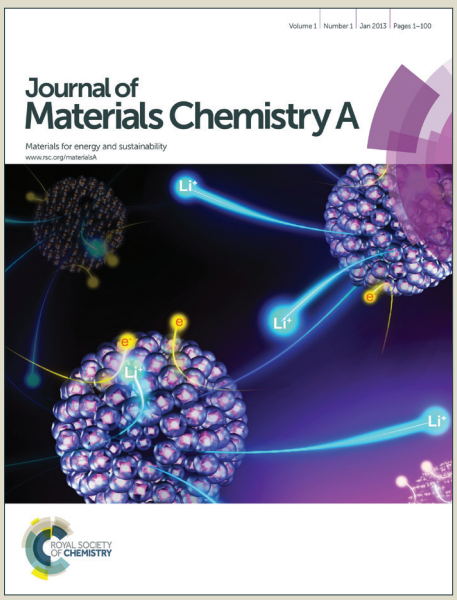

ROYAL SOCIETY OF CHEMISTRY

www.rsc.org/materialsA

Mg-TM (TM: Ti, Nb, V, Co, Mo or Ni) core-shell like nanostructures: Synthesis, hydrogen storage performance and catalytic mechanism

Jie Cui, Jiangwen Liu, Hui Wang, Liuzhang Ouyang, Dalin Sun*, Min Zhu*, Xiangdong Yao*

Correspondence information:

Dalin Sun: Department of Materials Science, Fudan University, Shanghai 200433, (P. R. China), dlsun@fudan.edu.cn;

Min Zhu: School of Material Science and Engineering, South China University of Technology, 510640, Guangzhou(P. R. China) , memzhu@scut.edu.cn;

Xiangdong Yao: Queensland Micro- and Nanotechnology Centre (QMNC), Griffith University, QLD 4111, Brisbane (Australia), x.yao@griffith.edu.au

Mg-TM (TM: Ti, Nb, V, Co, Mo or Ni) core-shell like nanostructures: Synthesis, hydrogen storage performance and catalytic mechanism

Jie Cui[a,b], Jiangwen Liu[a], Hui Wang[a], Liuzhang Ouyang[a],

Dalin Sun[c]*, Min Zhu[a]*, Xiangdong Yao[b]*

[a] School of Material Science and Engineering, South China University of Technology, Guangzhou, 510640, (P. R. China)

[b] Queensland Micro- and Nanotechnology Centre (QMNC), Griffith University, QLD 4111, Brisbane (Australia)

[c] Department of Materials Science, Fudan University, Shanghai 200433, (P. R. China)

Abstract:

Magnesium (Mg) was coated by different transition metals (TM: Ti, Nb, V, Co, Mo, or Ni) with a grain size of nano-scale to form a core (Mg)-shell (TM) like structure by a reaction of Mg powder in THF solution with $TMCl_x$. The thickness of the TM shell is less than 10 nm. TPD-MS result shows Mg-Ti sample can release hydrogen even under 200 ^oC. It is experimentally confirmed that the significance of catalytic effect on the dehydrogenation is in a sequence of Mg-Ti, Mg-Nb, Mg-Ni, Mg-V, Mg-Co and Mg-Mo. This may be contributed to the decrease of electro-negativity (χ) from Ti to Mo. However, Ni shows a special case with high catalytic effect in spite of the electro-negativity. It is supposed that the formation of Mg_2Ni compound may play an important role to enhance the hydrogen de/hydrogenation of Mg-Ni system. It can also be found that the larger formation enthalpy, the worse dehydrogenation kinetics.

Key Words: Hydrogen storage; transition metal, catalyst; mechanism

1. Introduction

Mg-based hydrides stand as a promising candidate for on-board hydrogen storage with reversible hydrogen capacity up to 7.6 wt%. However, it is well-known that the limitations are the thermodynamics stability (up to 300 ^{o}C for hydrogen release) and slow kinetics [1]. To overcome these barriers, tremendous efforts have been devoted to decrease the desorption temperature, enhance the kinetics and improve the cycle life in the past decades. Possible solutions to address these problems are the use of small nano-particles [2,3], alloying with transition metals [4,5], adding catalysts [6], or a combination of above approaches [7].

Recently, favor kinetic improvements and reduction in activation energies were obtained by the addition of palladium (Pd) [8], carbides [9] or carbon [10], but the most impressive results were obtained with transition metal catalysts such as titanium (Ti), niobium (Nb), vanadium (V), molybdenum (Mo), cobalt (Co), nickel (Ni), copper (Cu) and their respective compounds [11, 12, 13]. For example, Mg adding Co and multi-walled carbon nano-tubes (MCNTs) catalysts by ball-milling can absorb 6.5 wt% of H_2 after 100 s and desorb 5 wt% H_2 in 85 min at 250 °C [14]. Holtz and Imam reported an achievement of a decrease of onset temperature for hydrogenation from 275 °C to 175 °C by the addition of 1 at% of Ni to magnesium [15]. Han *et al* reported that MoS_2 and MoO_2 can also reduce the activation energy and ameliorate the hydriding/dehydriding kinetics of MgH_2 [16]. It was also reported hydrogen capacity can be increased up to 5.8 wt% under 300 ^{o}C within 15 min by adding V as a catalyst

[17]. Bazzanella *et al* achieved a remarkably enhancement of the hydrogen desorption/absorption kinetics with Nb or Nb_2O_5 additions [18,19]. Besides, Recham *et al* investigated MgH_2-2mol% NbF_5 system by different ball-milling parameters. They found better improvement was achieved by pre ball-milling the NbF_5 prior to direct addition to MgH_2, with a reduction of desorption activation energy from 88 to 72 kJ mol^{-1} [20]. Bhat *et al* reported that a nano-crystalline Nb_2O_5 with high specific surface area induces superior kinetics to commonly used Nb_2O_5 due to the larger contact area between Mg and Nb_2O_5 [21]. Similarly, a nano-composite of MgH_2-TiH_2 system by *in-situ* high energy ball-milling can release 6 wt % hydrogen at 300 °C in 10 minutes, which should be contributed to the sufficient interaction of nano-crystalline TiH_2 with MgH_2 [22,23]. All these indicate that the high surface area and morphology of the catalysts are important criteria in designing catalyst for hydriding/dehyriding of metal hydrides because it determines the catalytic interaction route and performance.

Beyond that, as the de/hydrogenation process is a gas-solid reaction whose reaction rate is affected significantly on the gas-solid interface [24], the most critical issue during the dehydrogenation process of MgH_2 is the H_2 molecule recombination on the surface of MgH_2. Hence, it is quite necessary to modify the surface of Mg/MgH_2, enabling the hydrogen recombination easier. Recently, many reports found the interesting features that Mg/MgH_2-M (M=Pd, RE and Ti or its compounds) nano-composites with modified surface show remarkably improvements in dehydrogenation properties [25,26]. For example, Higuchi *et al.* investigated three-layered Pd-Mg-Pd sandwich film fabricated

by an RF-associated magnetron sputtering methods and found that the desorption temperature could be lower than 100 °C [27]. They believed that the hydrogen atoms diffused from Mg matrix would be much easier to recombine on the Pd surface as Pd has the multiple valences that could facilitate the electron transfer between Mg^{2+} and H^-. Zou *et al* reported core-shell structured Mg-RE (RE=Nd, Gd, or Er) nano-composites improved hydrogen storage thermodynamic, kinetic and anti-oxidation properties as the solid solution state RE and the RE_2O_3 nano-grains covered on Mg surface [28]. Callini *et al* synthesized 2 at% Pd decorated Mg-MgO core-shell nano-particles which showed better ab/desorption behavior than Mg nano-particles themselves with the same size. However, the fabrication cost of such films and nano-particles is too high to be used practically, but this triggers an idea that coated a nano-layer of catalyst on the surface of traditional milled Mg powders that may also improve significantly the dehydrogenation of MgH_2.

In our recent studies, a nano-composite of Mg with a nano-coating of multi-valance Ti-based catalysts can release 5 wt % H_2 within 15 minutes under 250 ^oC, which contributes to the modified Mg surface by multiple Ti compounds with nano-grains [29]. We also have demonstrated that the catalytic effects of the composite lead to better acceleration of dehydrogenation kinetics than adding $TiCl_3$ by ball-milling. Notably, this study indicates that Mg with a nano-coating of transition metal compounds may be an effective strategy to significantly lower the desorption temperature and enhance the kinetics. In addition, the strategy is simple, low costly and easy to be scale-up. It is

therefore desirable to further explore and systematically investigate the effect of nano-coating of other transition metals on hydrogen storage behavior of Mg. The investigation is expected to provide a guidance to design such Mg-TM systems for hydrogen storage. In addition, it is also key to elucidate the mechanism of the transition metals coated on the surface of Mg. For the above reasons, we prepare a series of nano-composites (Mg-TM, TM=Ti, Nb, V, Co, Mo, Ni) by similar method in our recent work [29] and investigate the hydrogen storage behavior, which confirm the enhancement of hydrogen desorption from such core-shell like structured Mg-TM systems and propose plausible mechanism of catalytic effect.

2. Experimental Procedures

All experiments and handling were carried out in glove box in an argon atmosphere to prevent possible Mg oxidation. A series of samples named as Mg-Ti, Mg-Nb, Mg-V, Mg-Co, Mg-Mo and Mg-Ni were prepared by a reaction of the pre-milled Mg powder with corresponding chlorides ($TiCl_3$, $NbCl_5$, VCl_3, $CoCl_2$, $MoCl_3$, $NiCl_2$), separately. The detail experimental processes are shown in supporting information (SI). In order to characterize the structures, the phases were determined by a Philips X-ray diffract meter (XRD) with Cu-Kα radiation, the surface morphology was observed by a Nano430 scanning electron microscopy (SEM) and a JEM-2100 transmission electron microscope (TEM) operating at 200 kV, and the surface composition was characterized by an Axis Ultra DLD X-ray Photoelectron Spectroscopy (XPS). In addition, the temperaure programme desorption-mass spectrum (TPD-MS) was used to measure the hydrogen

desorption of the samples, by a heating equipment (Xian-quan Co., TP-5000) connected to a mass spectrometer (MS, Hiden, Qic 20) with a heating rate of 4 K min^{-1}. The hydrogen absorption and desorption properties can be tested by an automatic Sieverts apparatus (PCT Pro2000, Setaram, France). In present work, the isothermal hydrogenation and dehydrogenation curves were measured under 2 MPa and 1 kPa, at three different temperatures (225, 250, 275 °C), respectively.

3. Results and Discussion

3.1 Structure of Mg-TM samples

Fig. 1 shows XRD profiles for the Mg-TM samples in varying states (as-prepared, hydrogenated and dehydrogenated after 5 cycles.). It can be easily found that the as-prepared Mg-TM samples mainly contain Mg phase, and little of corresponding TM and $TMCl_x$/TMO_x phases. As shown in Fig. 1a, the as-prepared Mg-Ti sample mainly contains Mg and a small amount of Ti, TiO_2 and $TiCl_3$. The peaks of Ti and Ti-based compounds are all very relatively weak and broaden, which indicate that the particles are at nanoscale with a small amount. Similarly, other elemental TM peaks in the corresponding as-prepared Mg-TM samples are mainly weak and broaden. According to the XRD data, the grain size of TM in as-prepared Mg-TM samples can be estimated by the Scherrer equation (also referred to the Debye–Scherrer equation) [30] as shown in Eq. (1). The Scherrer equation relates the width of a powder diffraction peak to the average (by volume) dimensions of crystallites in polycrystalline powders:

$$\beta_s(2\theta)_{hkl} = \frac{K\lambda}{T\cos\theta_{hkl}} \quad \text{Eq(1)}$$

where β_s is the crystallite size contribution to the peak width (integral or full width at half maximum) in radians, K is a constant near unity, and T is the average thickness of the crystal in a direction normal to the diffracting plane $h\ k\ l$. The value of K is slightly different depending upon whether the full width at half maximum or the integral width is chosen to characterize the peak breath. According the XRD data in the present work, the grain size of TMs are in a range of 9~20 nm as shown in Table 1. As the particle size is around 500-1000 nm, a particle contains thousands of such grains with tremendous grain boundaries. The grain boundaries may be beneficial for atomic hydrogen diffusion and act as active sites for hydride formation, resulting in the enhancement of hydrogenation/dehydrogenation. After hydrogenation, Mg transforms into MgH_2. As shown in Fig. 1a, Ti phase in as-prepared Mg-Ti sample changes into TiH_2 after hydrogenation, and TiH_2 peak still remains after dehydrogenation. However, Ni in as-prepared Mg-TM sample transforms into Mg_2NiH_4 after hydrogenation, and Mg_2NiH_4 transforms into Mg_2Ni after dehydrogenation as shown in Fig. 1e. According to the XRD patterns shown in Fig. 1b, c, d and f, unlike Mg-Ti and Mg-Ni samples, other TM (Nb, V, Co and Mo) and $TMCl_x$ ($NbCl_5$, VCl_3, $CoCl_2$ and $MoCl_3$) are existed in Mg-Nb, Mg-V, Mg-Co and Mg-Mo samples during the hydrogenation and dehydrogenation process without phase transformation. It is not surprising because Nb and V can serve as "hydrogen pump". This means that the H on Nb and V can be easily transferred to neighboring Mg. As compared to Mg, the amount of Nb and V is limited. Accordingly, the hydrides of Nb and V may be only in a trace amount, which can not be

detectable the use of XRD. Co and Mo are hard to form hydrides.

To observe the surface morphology of the Mg-TM samples, high magnification SEM is employed and the images are shown in Fig. 2. It illustrates that small uneven protuberances with different sizes (about 10~50 nm) are shown on the surface of the particles. The protuberances should be the reserved products after the reaction of Mg with the corresponding $TMCl_x$ in solution. Combined with the XRD results of the as-prepared Mg-TM samples, it can be infered that the small protuberances coated on the surface of Mg particles are corresponding to TM and TM-based chlorides. These morphology features are similar with the morphology of Mg-Ti, which has been clarified as a nano-coating of multi-valence Ti-based catalyst [29]. Hence, it implies that the TM-based catalysts are covered on the Mg surface in Mg-TM samples, like the case of Mg-Ti.

As the coating microstructures of Mg-Nb (V, Co, Mo) may be similar to Mg-Ti, we will not deliver the further TEM observations on these samples. However, Mg-Ni is an exceptional case as the new Mg_2Ni phase will be formed during the de/hydrogenation and this Mg_2Ni phase is supposed to be important for the hydrogen storage behavior. Therefore, we employed TEM observations of the hydrogenated Mg-Ni sample and the results are shown in Fig. 3. Fig. 3a gives the TEM bright image of the hydrogenated Mg-Ni sample. It is can be found that the edge section shows a deeper contrast, indicating a core/shell like structure. Table 2 gives the results of micro-area EDS analysis in different square areas as shown in Fig. 3a. According to the EDS results in

Table 2, it is easy to find that the contents of Ni in area 1, 2, 3 and 4 (in shell area) reach up to ~37 wt%, which is far higher than that of area 5 and 6 (in matrix). This supports that the Ni-based materials are covered on the surface of Mg, in accordance with the observations of SEM (Fig. 2). Besides, the selected area electron diffraction (SAED) patterns of the circle area (shown in Fig. 3b) confirm that the shell contains $NiCl_2$, NiO, Mg_2Ni and MgH_2. In the hydrogenated Mg-Ni sample, we can only observe Mg_2Ni but not Mg_2NiH_4. This may because Mg_2NiH_4 releases hydrogen under the electron illumination of 200 kV and high vacuum during TEM observations. In addtion, $NiCl_2$ and NiO are confirmed in TEM but not in XRD patterns, which may be due to undetectable amount of $NiCl_2$ and NiO by XRD. The extistence of $NiCl_2$ and NiO can be also confirmed in later by XPS. Fig. 3c also demonstrates that the thickness of the shell is less than 10 nm.

The bonding state analysis was measured by XPS. All the signals in hydrogenated samples are very weak but detectable. It is suggested that the shell of all samples contain transition metals, metal chlorides and oxides. As an example in Fig. 4, both the hydrogenated and dehydrogenated Mg-V sample after 5 cycles show V 2p signals of V, VCl_3, VO_2 and V_2O_5 although the peak of V 2p signals are weaken. The formation of vanadium oxide may be due to the oxidation during the sample preparation. Similar with Mg-V samples, Nb 3d signals of Nb, $NbCl_5$, NbO and Nb_2O_5 appear both in the hydrogenated and dehydrogenated Mg-Nb sample after 5 cycles as shown in Fig. 1S in SI. Co 2p signals of Co, $CoCl_2$ and CoO can be detected both in the hydrogenated and

dehydrogenated Mg-Co sample after 5 cycles as shown in Fig. 2S in SI. These results suggested again that the shell structures are almost same as that of Mg-Ti [29], thus the TEM observations can be neglected. However, Mg-Ni is an exceptional case. Fig. 3S gives that Ni 2p signals of Ni, $NiCl_2$ and NiO exsit in the as-prepared Mg-Ni sample, but after hydrogenation, Ni 2p signal of Ni dispeared. Combinated with the XRD and TEM, it can be suggested that Mg_2NiH_4 is formed after hydrogenation. This can also be proved by the left shifting of Mg 1s signal as shown in Fig. 4S in SI, which stands for the metallic state of Mg formed [31].

Accordingly, it can be inferred that the core/shell like stuctures have been formed by Mg reaction with TM chlorides in all Mg-TM samples. In Mg-Ti, Mg-V, Mg-Nb, Mg-Co and Mg-Mo samples, the "shell" contains corresponding elemental TM, chloride and oxide with a chickness of ~10 nm covered on the surface of Mg/MgH_2 as the "core". In Mg-Ni samples, the shell of as-prepared sample also contains Ni, $NiCl_2$ and NiO, similar to other Mg-TM systems. When hydrogenated, however, unlike the TM remains unchanged in other Mg-TMs, Ni in Mg-Ni disappears and forms Mg_2Ni. It is supposed that the coated TM (other than Ni) play a similar role in enhancing the hydrogen storage of Mg as Ti in Mg-Ti, but Ni will be different as the *in situ* formed Mg_2Ni will also take a significant effect on hydrogen storage of Mg-Ni system.

3.2 Hydrogenation/dehydrogenation performance

The hydrogenation of Mg-TM samples has been performed at three different temperatures of 225, 250, and 275 °C, respectively. All samples show favor

hydrogenation kinetics. As can be seen in Fig. 5a, the Mg-Ti sample can absorb 4.1, 4.9 and 5.5 wt% hydrogen in 5 minutes s at 225, 250 and 270 °C, respectively. As shown in Fig. 5b, the Mg-Nb sample can absorb 4.2, 5.4 and 5.85 wt% in 5 minutes, respectively. Under the same conditions, the Mg-V sample can absorb 3.47, 4.9 and 5.5 wt% hydrogen in 5 minutes, respectively. The Mg-Co sample can absorb 4.0, 4.5 and 5.5 wt% hydrogen, respectively. The Mg-Mo sample can absorb 3.0, 4.0 and 4.8 wt% hydrogen, respectively. The Mg-Ni sample shows the fastest hydrogenation rate, which can absorb 6.2 wt% hydrogen in 1 minute at 275 °C, 6.0 wt% in 5 minutes at 250 °C and 5.75 wt% in 5 minutes at 225 °C, respectively. It is well known that the kinetics of hydrogen absorption in magnesium is affected by two main activation processes: the dissociation of the H_2 molecule and the diffusion of atomic H into the bulk. DFT calculations suggested that the dissociation of the H_2 molecule can be promoted by adding transition metals (Ti, Zr, V, Fe, Co, Ni, Pd, Cu, Mo) on Mg surfaces [32,33]. Hence, it is not surprised that Mg-TM samples show good hydrogenation performance. In addition, it can be found the hydrogenation performance is in a sequence of Mg-Ni, Mg-Nb, Mg-Ti, Mg-V, Mg-Co and Mg-Mo. Pozzo *et al* pointed out that Ni is the best choice for hydrogen absorption, combining low activation barriers for the two processes by DFT calculations. Hence, the best hydrogenation of Mg-Ni in this experiment supports the theoretical calculations.

Another side, the dehydrogenation performance, is more critical as higher temperature is necessary to desorb hydrogen than adsorb hydrogen in Mg. Fig. 6 shows

the desorption of Mg-TM samples by TPD-MS. The desorption temperatures of all Mg-TM samples reduce significantly compared to the temperature of ball-milled MgH_2 (376 °C). The peak temperature of hydrogen desorption in Mg-TM samples is in a sequence of Mg-Ti (225 °C), Mg-Nb (244 °C), Mg-Ni (245 °C), Mg-V (282 °C), Mg-Co (288 °C) and Mg-Mo (304 °C). Obviously, Ti is the best for hydrogen desorption from MgH_2, which can reduce a temperature of ~150 °C compared to milled MgH_2. It is also observed that there is a small peak at 100 °C in each of the curves, reflecting the evaporation of little unavoidable water introduced during the sample transportation, and this can be ignored.

Fig. 7 shows the dehydrogenation kinetic curves measured for Mg-TM samples at desorption temperatures of 275, 250, and 225 °C, respectively. The Mg-Ti sample can release 6.35, 4.6 and 2.5 wt% hydrogen in 10 minutes at 275, 250, and 225 °C, respectively. In contrast, ball-milled Mg-$TiCl_3$ can only release 3.6 wt% H_2 and 1.0wt % H_2 in the same time at 275 and 250 °C, respectively, and can not release hydrogen at 225 °C. As shown in Fig. 7b, the Mg-Nb sample can desorb 3.75, 2.5 and 1.0 wt% hydrogen in 10 minutes at 275, 250, and 225 °C, respectively. However, ball-milled MgH_2-0.4 mol% $NbCl_5$ system can only desorb 5.2 wt% in 50 min at 300 °C by Bhat *et al* [34]. The Mg-V sample can release 3.1, 1.1 and 0.75 wt% hydrogen in 10 minutes at 275, 250, and 225 °C as shown in Fig. 7c. The Mg-Co sample can release 2.0, 0.7 and 0.4 wt% hydrogen in 10 minutes at 275, 250, and 225 °C, respectively as shown in Fig. 7d, which is much faster than the kinetics of Mg ball milled with Co (with various sizes)

and CoO by Lee *et al* (only can desorb 1 wt% hydrogen under 325 °C within the same time) [35]. The Mg-Ni sample can desorb 3.6, 2.0 and 0.8 wt% hydrogen in 10 minutes at 275, 250, and 225 °C, respectively as shown in Fig. 7e. The Mg-Mo sample can release 1.0, 0.5 and 0.1 wt % hydrogen in 10 minutes at 275, 250, and 225 °C as shown in Fig. 7f. From the current experimental results, it can be concluded that the coated Mg-TM is much superior to traditional ball-milled corresponding TM (or TM chlorides/oxides) with Mg in dehydrogenation. Among them, Ti is the best and followed by Nb.

To further study the dehydrogenation kinetics, the activation energy (E_A) for dehydrogenation was determined. In this study, the activation energy (E_A) for dehydrogenation of Mg-TMs evaluated from the Arrhenius plot of rate constant k values with temperature by simply plotting a straight line ln(k) vs. 1/ RT.

$$k = k_0 e^{-E_A/RT} \quad \text{Eq(2)}$$

As shown in [eq (2)], E_A is the apparent activation energy, R is the gas constant (8.314472 J $mol^{-1}K^{-1}$), and T is the Kelvin temperature. Several solid-state reaction mechanism models have been tested to select the best fitting form, including the nucleation and growth, geometric contraction, diffusion, and the reaction order models based on the different geometry of the particles and the different driving forces. As shown in [eq (3)] where the symbol α is the fraction of Mg transformed from MgH_2 at time t, the function based on geometric contracting volume (R3 model) gives the best results:

$$kt = 1 - (1 - \alpha)^{1/3} \quad \text{Eq(3)}$$

Fig. 8 shows the Arrhenius-type plots for the above six samples for comparison, the values of E_A for these samples are given in Table 3, which obviously shows the following: (1) all the Mg-TMs improve significantly the dehydrogenation kinetics (reduction of E_A); (2) the Mg-TM are more efficient than ball-milled Mg-TM systems; and (3) the ability for promoting the dehydrogenation kinetics can be ranked as Mg-Ti, Mg-Nb, Mg- Ni, Mg-V, Mg-Co and Mg-Mo according the E_A.

3.3 Dehydrogenation Mechanism

Hydrogenation/dehydrogenation process is a gas-solid reaction whose reaction rate is affected significantly on the gas-solid interface. In the present work, it is proved that nano-crystallite TM-based catalysts with multi-valences are covered on the surface of Mg particles. Hence, the surface of Mg/MgH_2 is modified by the "shell" of catalysts, which can be regarded as *surface contact* between Mg/MgH_2 and nano-crystalline TM. This is completely different from the *point contact* of Mg/MgH_2 with TM-based catalyst by ball milling. A schematic diagram shows the different effect of two types of contacts as seen in Fig. 9. Fig. 9a shows the current systems by TM-based catalyst covered on the surface of Mg/MgH_2. $TM^{x/y}$ stands for the multi-valences of TM-based catalyst in which x/y refers to the valence state of TM. This kind of surface contact structure leads to almost all the Mg^{2+} and H^- on the surface of MgH_2 are interacted with the TM-based catalyst as shown in the middle of Fig. 9a. For comparison, the point contact of Mg/MgH_2 with TM-based catalyst by ball-milling can be schematically drawn in Fig.

9b. In this case, only part of H^- ions on the surface of MgH_2 can be interacted with the $TM^{x/y}$ ions. Due to the *d* orbital's characteristics of TM, $TM^{x/y}$ ions can loss or get electrons more easily than Mg^{2+}, then act as the electron transfer medium during the hy-/dehydrogenation process. Hence, it can be inferred that all the Mg-H bonding on the surface are affected by the whole cover of $TM^{x/y}$ and thus weakened. Therefore, dehydrogenation process in Mg-TM system can be proposed as the following steps: (1) $2H^-$ on the interface between MgH_2 and TM-based catalyst diffuse into the shell to form TM-H bonds, simultaneously, two electrons from TM transfer (valence of TM is changed) to Mg^{2+} to Mg. Mg nucleates and grows when this process is continuing; (2) H^- diffuses across the nano-shell of TM-based catalyst and arrives on the surface; (3) Break of TM-H bonds. two H^- losts two electrons to form H^0 and these two H^0 recombine into H_2 molecule on the surface of TM-based catalyst. At the same time, TM gains two electrons (valence of TM is changed back). This is a redox like mechanism in which the multi-valence TM serves as a medium for electron transfer. With this mechanism, the hydrogen desorption only relates to hydrogen H^- diffusion in MgH_2 matrix, H^0 across the Mg/TM and recombination of H_2 on TM surface. It is well known that the energy barrier for atomic hydrogen diffusion is relatively lower and not the key barrier for hydrogen desorption. The limit for hydrogen desorption is the recombination and release of H_2 from Mg surface. It is supposed that the energy barrier for hydrogen recombination and release from TM catalyst is significantly lower, thus the cover of TM on Mg surface avoids the high energy barrier. Accordlingly, the hydrogen desorption of

Mg-Tm becomes easier.

However, the point contact by ball-milling Mg-based system takes only part of this effect as shown in Fig. 9b. We can roughly estimate the effective part of this type of contacts. Given a particle size of Mg sample is 1 μm, and supposed an average size of 200 nm of TM particles embedded in Mg particles, and assumed an embedded angle of 180°, it can be estimated that the catalyst contact area is about 1/6 of the whole covered surface with a same adding level (half of them appears on the surface of Mg). Accordingly, the effective sites of Mg-TM systems for hydrogen desorption are assumed to be 6 times more than those in the ball-milled samples. This may be one of the reasons why Mg-TM exhibits superior hydrogen desorption performance.

As the mechanism of hydrogen desorption of Mg-TM is depended on the electron transfer through a bridge of multi-valence TM, the ability of loss and gain electrons of different TMs should be a key factor to influence the catalytic effect. The electro-negativity (χ) of TM represents the ability of losing or getting electron of TM or TM ions. Fig. 10a and b show the relationship of hydrogen release kinetics and activation energy with χ. In Fig. 10a, it is very interesting to obtain that the hydrogen release rate is decreased with the increase of χ but Ni is an exceptional. It is also seen that the E_A is decreased with the increase of χ except the Mg-Ni system.

In this mechanism, the control step is the broken of TM-H bonds. As the ability of metals losing/gaining electrons is decreased with the increase of χ. This means that metals bind with H stronger in a decrease of χ. Therefore, it is reasonable that Mg-Ti

shows the best dehydrogenation performance as Ti is with the smallest χ. Besides, as Ti has a similar atomic size with Mg, it is likely that some of Mg atoms in the cell may be replaced by Ti, resulting in some deformation of the MgH_2 structure on the interface. This deformation may cause strains that provide higher energy state of Mg-Ti, so the energy barrier for hydrogen desorption may alter to smaller. It is also possible that this deformation may lead to the presence of more vacancies that are favorable for the atomic hydrogen diffusion.

Mg-Ni system shows difference from other Mg-TM systems due to formation of Mg_2Ni. It is reported that Mg_2Ni is easy to combine with H to form Mg_2NiH_4. Fortunately, Mg_2NiH_4 is also much easier to release hydrogen compared with MgH_2 (the enthalpy of formation for $Mg_2NiH_4$is ~40kJ/molH_2, which is almost half for Mg) [36, 37]. Therefore, the widely dispersed, *in situ* formed and very fine Mg_2Ni in MgH_2 matrix can serve as so-call "hydrogen pump" that significantly facilitate hydrogen diffusion. More importantly, the easier release of H from Mg_2NiH_4 enables the H^- transfers to TM on Mg_2NiH_4/TM interface much easier. This is extra effect for hydrogen desorption of Mg-Ni system than other Mg-TM systems without formation of another phase of high hydrogen affinity like Mg_2Ni. Therefore, Mg-Ni is an exceptional of χ rule for hydrogen desorption. The interaction intension of transition metals with hydrogen can be represented by the formation enthalpy of transition metal hydrides. It is believed that the larger formation enthalpy, the stronger interaction between transition metals and hydrogen. Hence, according the formation enthalpy data reported in

Suzuki's work [38], the relationship between the formation enthalpy and E_A can be plotted as Fig. 11. It can be found that E_A increase with the increase of formation enthalpy.

Conclusion

A series of nano-composites (Mg-TM, TM=Ti, Nb, V, Co, Mo, Ni) prepared by a reaction of Mg powder with $TMCl_x$ show favorable dehydrogenation performance. All systems can release hydrogen at a low temperature at 225 ^oC. This study illustrates that the nano-coating of TM around the surface of MgH_2 is much more effective than traditional ball-milling Mg with corresponding TMs. The ability for promoting the dehydrogenation kinetics (high kinetic rate and small E_A) can be ranked as Mg-Ti, Mg-Nb, Mg- Ni, Mg-V, Mg-Co and Mg-Mo. A plausible dehydrogenation mechanism was proposed to understand the dehydrogenation with TMs. The hydrogenation performance is better with smaller electro-negativity. However, Mg-Ni is an exceptional due to the *in situ* formation of fine Mg_2Ni with high hydrogen affinity.

Acknowledgments

This work was financially supported by Australian Research Council (ARC), the Ministry of Science and Technology of China (No. 2010CB631302).

Reference

[1] Mushnikov NV, Ermakov AE, Uimin MA, Gaviko VS, Terent'ev PB, Skripov AV, Tan AP. Phys Met Metall 2006; 102:421.

[2] Jeon KJ, Moon HR, Ruminski AM, Jiang B, Kisielowski C, Bardhan R, Urban JJ. Nat Mater 2011; 10: 286

[3] Choi YJ, Choi JW, Sohn HY, Ryu T, Hwang KS, Fang ZZ. Int J Hydrogen Energy 2009; 34:7700.

[4] Hirscher M, Becher MJ. J Nanosci Nanotechnol 2003; 3: 3.

[5] Skripnyuk VM, Rabkin E, Estrin Y, Lapovok R. Int J Hydrogen Energy 2009; 34:6320.

[6] Barkhordarian G, Klassen T, Bormann R. Scr Mater 2003; 49:213.

[7] Oelerich W,Klassen T, Bormann RJ. Alloys Compd 2001; 15:237.

[8] Renaud D, Sébastien M, Marc S, Joris P. Acta Materialia 2013; 61: 2320.

[9] Reda MR. J Alloys Compd 2009; 480:238.

[10] Shang CX, Guo ZX. J Power Sources 2004; 129:73.

[11] Barkhordarian G, Klassen T, Bormann R. J PhysChem B 2006; 110:11020.

[12] JiaY, Cheng L, Pan N, Zou J, Lu GQ, Yao XD. AdvEner Mater 2011; 1:387.

[13] Liang G, Huot J, Boily S, Van Neste A, Schulz R. J Alloys Compd 1999; 292:247.

[14] Verón MG, Troiani H, Gennari FC. Carbon. 2011; 49: 2413.

[15] Holtz RL, Imam MA. J Mater Sci 1999; 34:26:55.

[16] Jia YH, Han SM, Zhang W, Zhao X, Sun PF, Liu YQ, Shi H, Wang JS. Int J Hydrogen Energy 2013; 38:2352.

[17] Barkhordarian G, Klassen T, Bormann R. Scr Mater 2003; 49:213.

[18] Bazzanella N, Checchetto R, Miotell A, Sada C, Mazzoldi P, Mengucci P. Appl Phys Lett 2006; 89:014101.

[19] Huot J, PelletierJF, LiangG, SuttonM, SchulzR. J AlloysCompd 2002; 330:727.

[20] RechamN, BhatVV, KandavelM, AymardL, TarasconJM, RougierA.J Alloys Compd 2008; 464:377.

[21] Bhat VV, Rougier A, Aymard L, Nazri GA, Tarascon JM. . J Alloys Compd 2008; 460:507.

[22] Lu J, Choi YJ, Fang ZZ, Sohn YH, Ewa R. J Am ChemSoc 2009; 131:15843.

[23] Lu J, Choi YJ, Fang ZZ, Sohn YH, Ewa R. J Am ChemSoc 2010; 132:6616.

[24]Aguey-Zinsou K,Ares-Fernández J. Ener Environ Sci 2010; 3:526.

[25] Higuchi K, Kajioka H, Toiyama K, Fujii H, OrimoS, Kikuchi Y. J Alloys Compd 1999; 293:484.

[26] Borgschulte A, Rector JH, Schreuders H, Dam B, Griessen R. Appl Phys lett 2007; 90:071912.

[27] Higuchi K, Yamamoto K, Kajioka H, Toiyama K, Honda M, Orimo S, Fujii H. J Alloys Compd 2002;330,526.

[28] Zou JX, Zeng XQ, Ying YJ, Chen X, Guo H, Zhou S, Ding WJ. Int J Hydrogen Energy 2013; 38:2337.

[29] Cui J, Wang H, Liu JW, Ouyang LZ, Zhang QA, Sun DL, Yao XD, Zhu M. J Mater Chem A 2013; 1:5603.

[30] Scherrer P, Gottingen NGW, Math-Pys Kl 1918; 2:96.

[31] Tajima K, Hoota H, Yamada Y, Okada M, Yoshimura K. Sol Energ Mat Sol C 2011; 95:3370.

[32] Tsuda M, Agerico Diño W, Kasai H, Nakanishi H, Aikawa H. Thin Solid Films 2006; 509: 157.

[33] Kobayashi T, Takasaki A. J Alloys Compd 2013; 580: 229

[34] Bhat VV, Rougier A, Aymard L, Darok X, Nazri G, Tarascon JM. J Power Sources 2006; 159: 107.

[35] Lee DS, KwonI H, Bobet JL, Song MY. J Alloys Compd 2004; 366(1-2):279.

[36] Chitsaz KL, Raygan SH, Pourabdoli M. Int J Hydrogen Energy 2013; 38:6687.

[37] Mao JF, Guo ZP, Yu XB, Liu HK, Wu Z, Ni J. Int J Hydrogen Energy 2010; 35: 4569.

[38] Suzuki K. J Less-Common Met. 1983; 89:183.

Figure Captions

Fig. 1 The XRD profiles for the Mg-TM samples in varying states (as prepared, hydrogenated and dehydrogenated after 5 cycles.). a: Mg-Ti; b: Mg-Nb; c: Mg-V; d: Mg-Co; e: Mg-Ni; f: Mg-Mo.

Fig. 2 The SEM images of the as prepared Mg-TM samples. a: Mg-Ti; b: Mg-Nb; c: Mg-V; d: Mg-Co; e: Mg-Ni; f: Mg-Mo.

Fig. 3 TEM micrograph of the hydrogenated Mg-Ni sample.

Fig. 4 V 2p photo electron lines for the hydrogenated and dehydrogenated Mg-Ni samples, after 5 cycles, repectively.

Fig. 5 Isothermal hydrogenation curves of Mg-TM samples at 225, 250, and 275 °C. a: Mg-Ti; b: Mg-Nb; c: Mg-V; d: Mg-Co; e: Mg-Ni; f: Mg-Mo.

Fig. 6 TPD-MS curves of Mg-TM samples with a heating rate of 4 $Kmin^{-1}$.

Fig. 7 Isothermal dehydrogenation curves of Mg-TM samples at 225, 250, and 275 °C. a: Mg-Ti; b: Mg-Nb; c: Mg-V; d: Mg-Co; e: Mg-Ni; f: Mg-Mo.

Fig. 8 Arrhenius plots of the desorption rate for the Mg-TM samples

Fig. 9 The section schematic diagram of Mg-TM and ball-milled Mg-TM-based catalyst

Fig. 10 a: Comparison in dehydrogenation average kinetics within 5 minutes of Mg-TM samples at 225, 250 and 275 °C; b: The plot of E_A vs χ of TM in Mg-TM systems.

Fig. 11 The plot of E_A vs formation enthalpy of TMH_x in Mg-TM systems.

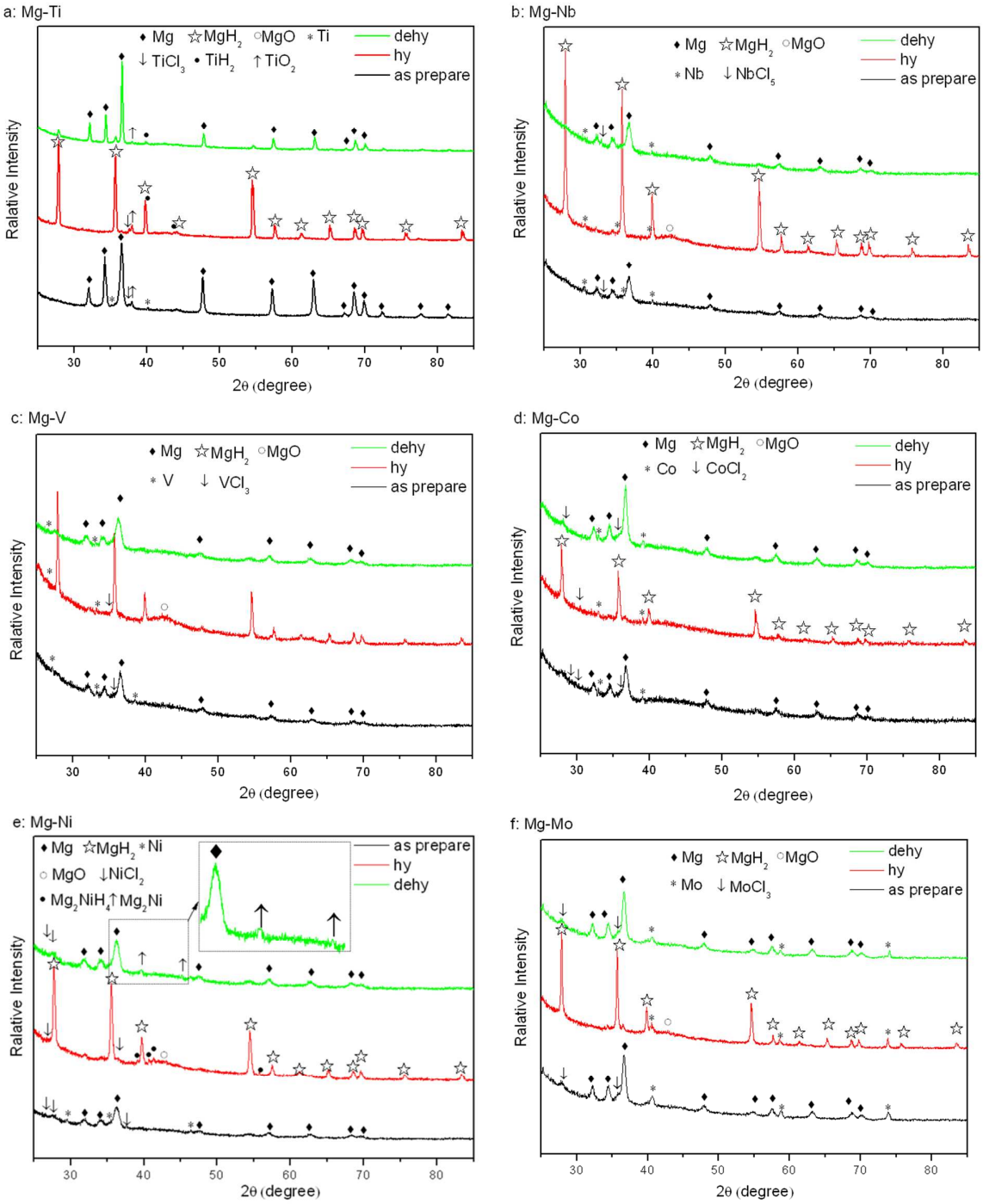

Fig. 1 The XRD profiles for the Mg-TM samples in varying states (as prepared, hydrogenated and dehydrogenated after 5 cycles.). a: Mg-Ti; b: Mg-Nb; c: Mg-V; d: Mg-Co; e: Mg-Ni; f: Mg-Mo.

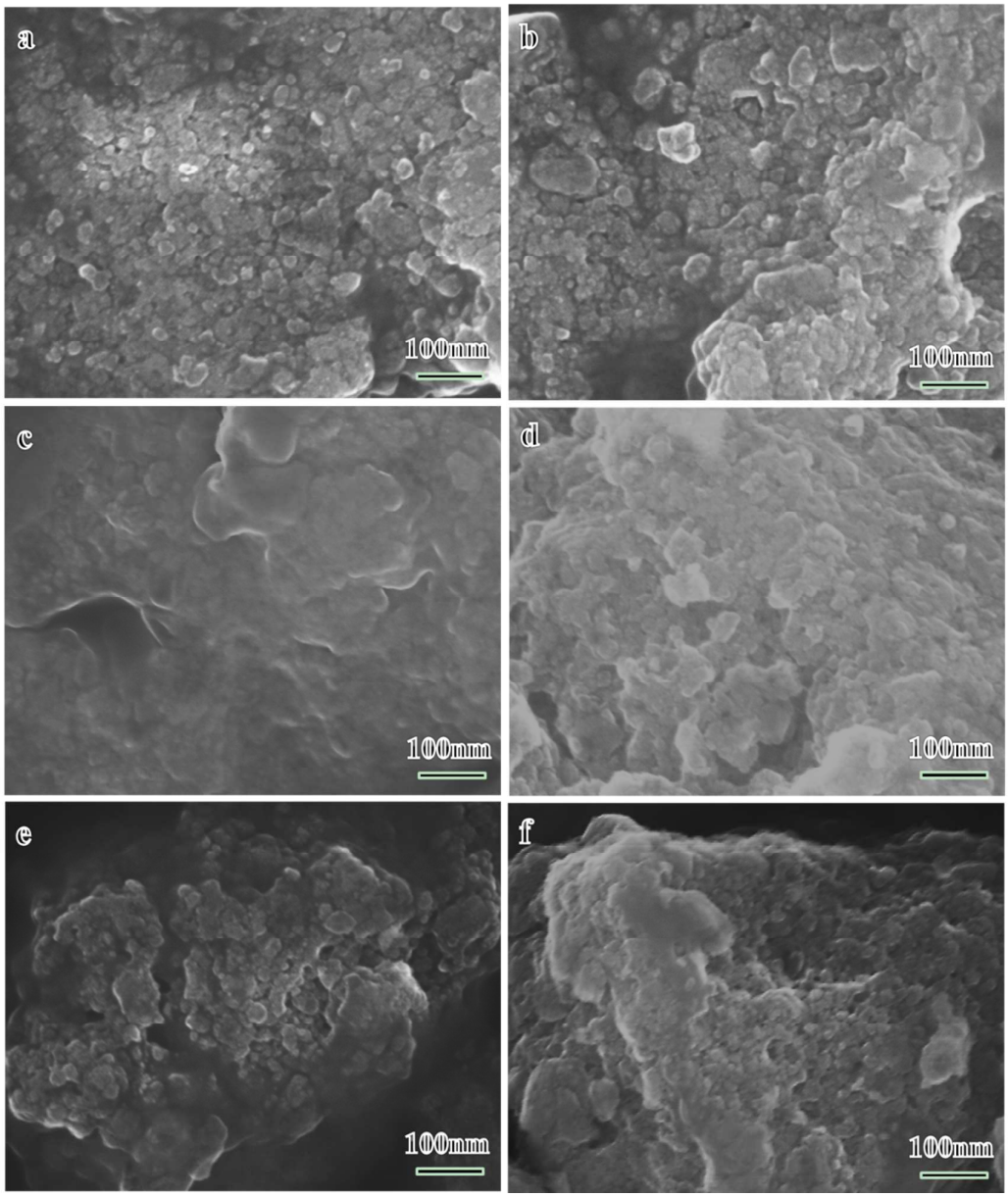

Fig. 2 The SEM images of the as prepared Mg-TM samples. a: Mg-Ti; b: Mg-Nb; c: Mg-V; d: Mg-Co; e: Mg-Ni; f: Mg-Mo.

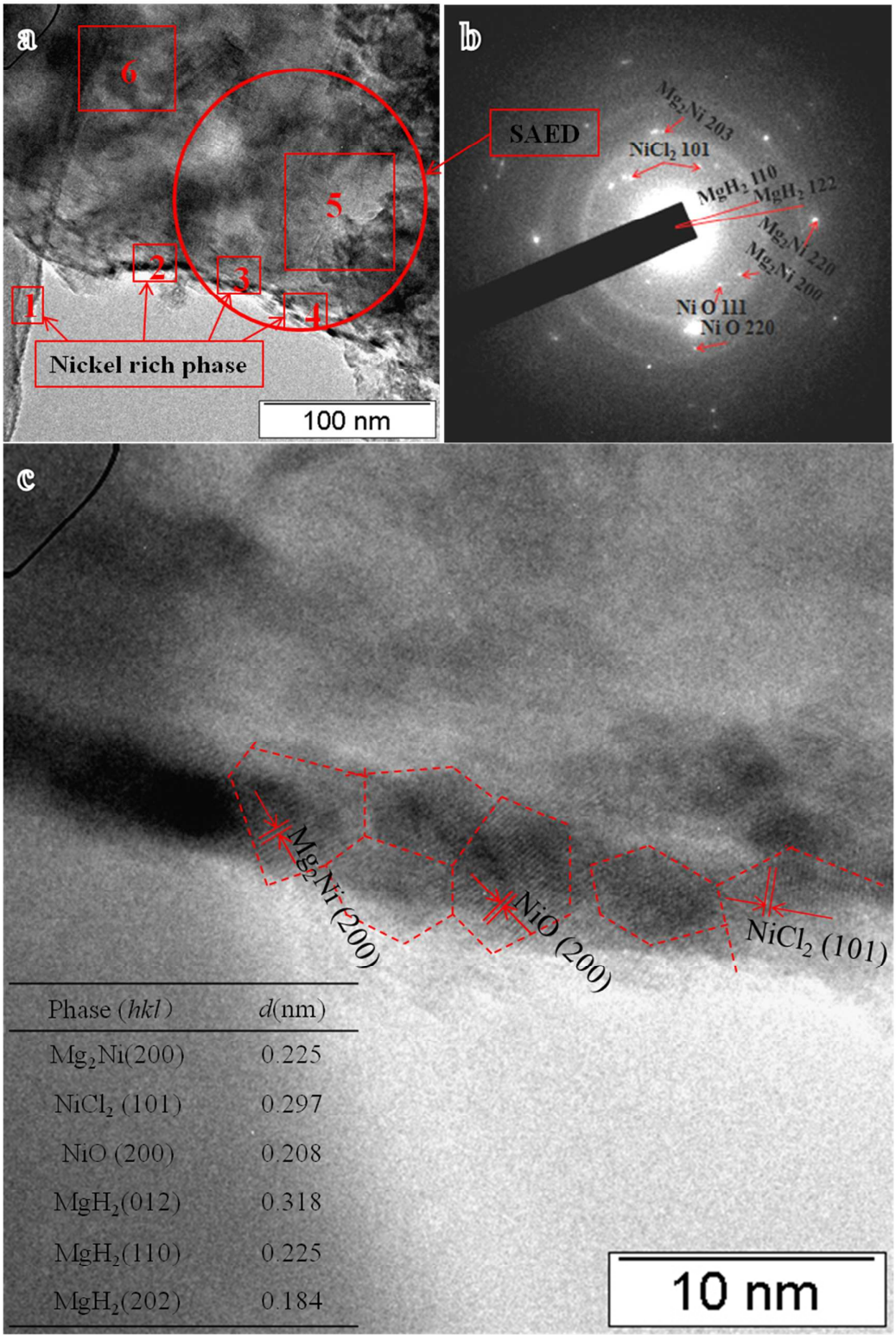

Phase (*hkl*)	*d*(nm)
Mg_2Ni(200)	0.225
$NiCl_2$ (101)	0.297
NiO (200)	0.208
MgH_2(012)	0.318
MgH_2(110)	0.225
MgH_2(202)	0.184

Fig. 3 TEM micrograph of the hydrogenated Mg-Ni sample. a: Bright field; b: Electron diffraction pattern; c HR-TEM images

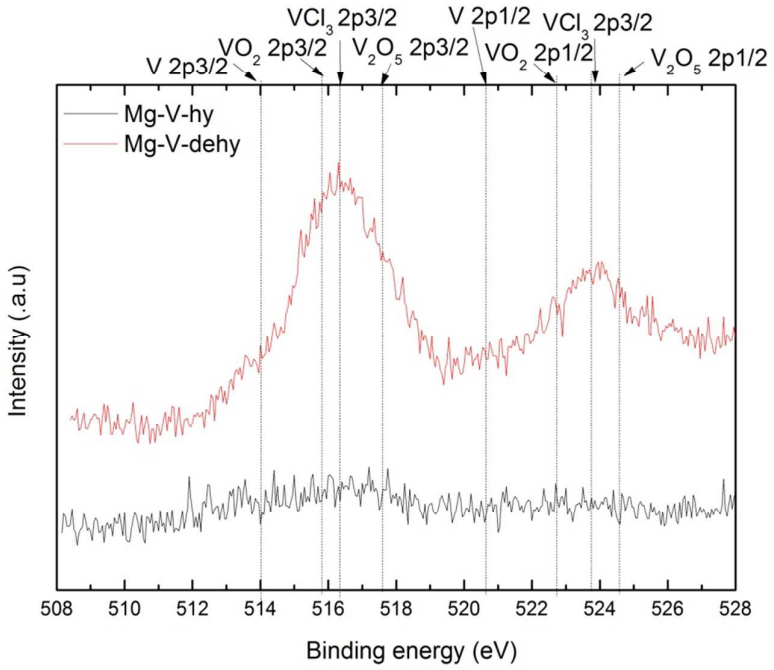

Fig. 4 V 2p photo electron lines for the hydrogenated and dehydrogenated Mg-Ni samples, after 5 cycles, repectively.

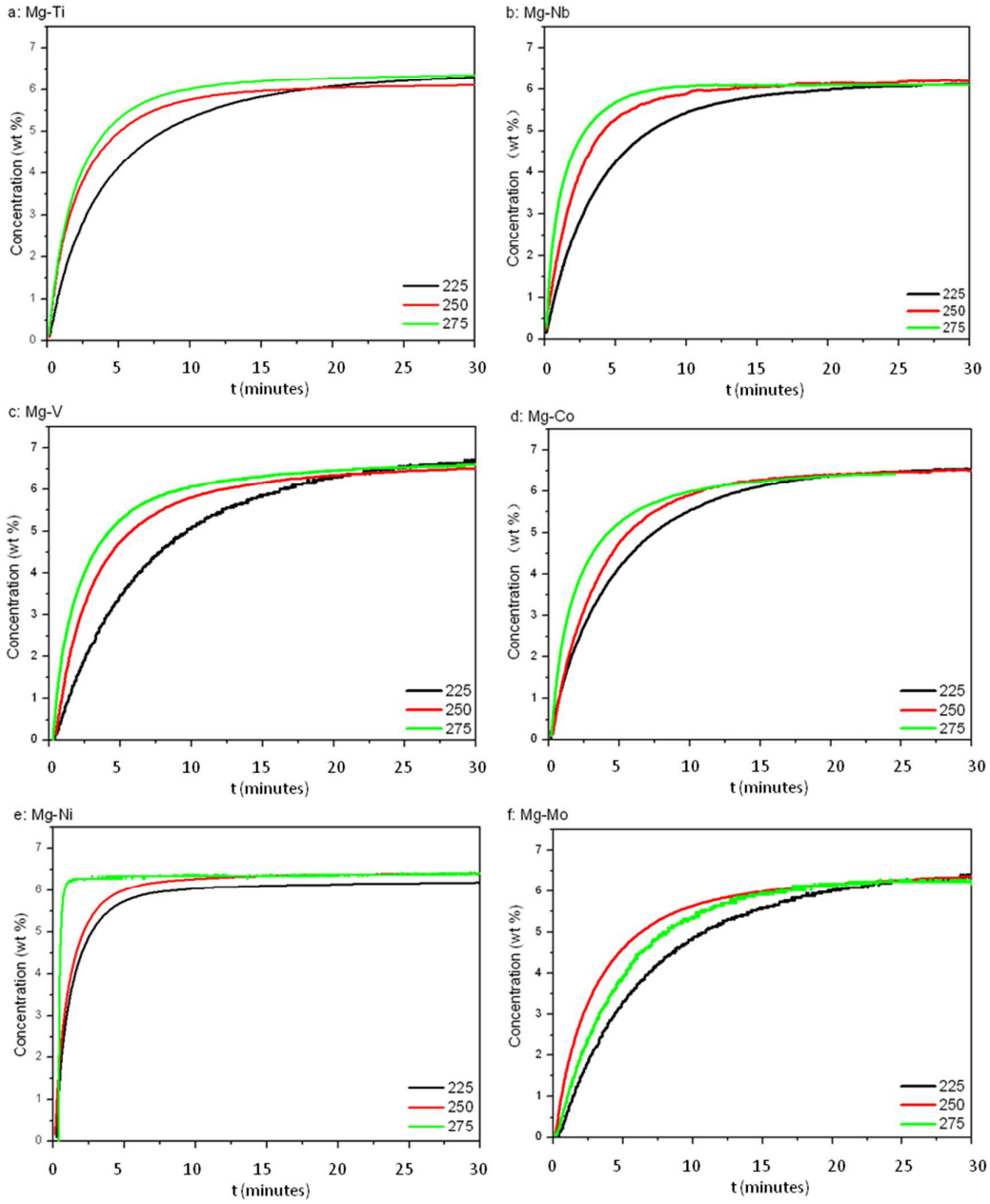

Fig. 5 Isothermal hydrogenation curves of Mg-TM samples at 225, 250, and 275 °C. a: Mg-Ti; b: Mg-Nb; c: Mg-V; d: Mg-Co; e: Mg-Ni; f: Mg-Mo.

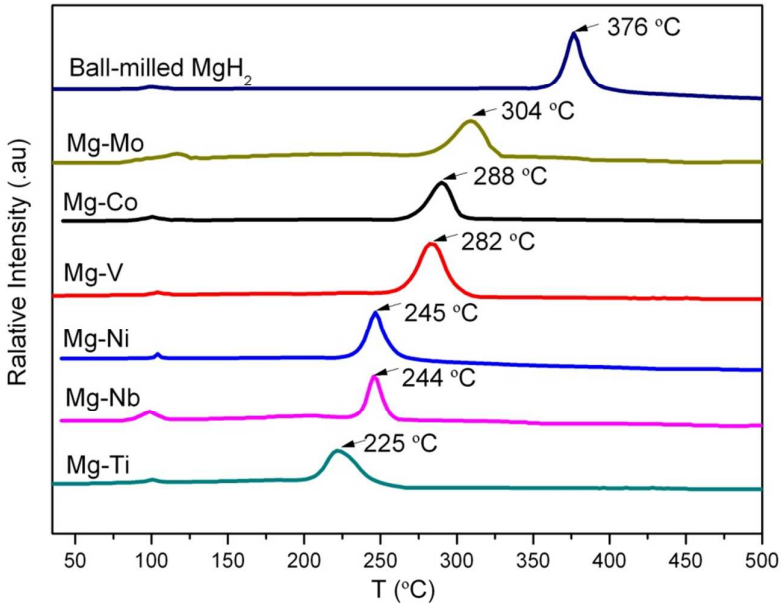

Fig. 6 TPD-MS curves of Mg-TM samples with a heating rate of 4 $Kmin^{-1}$.

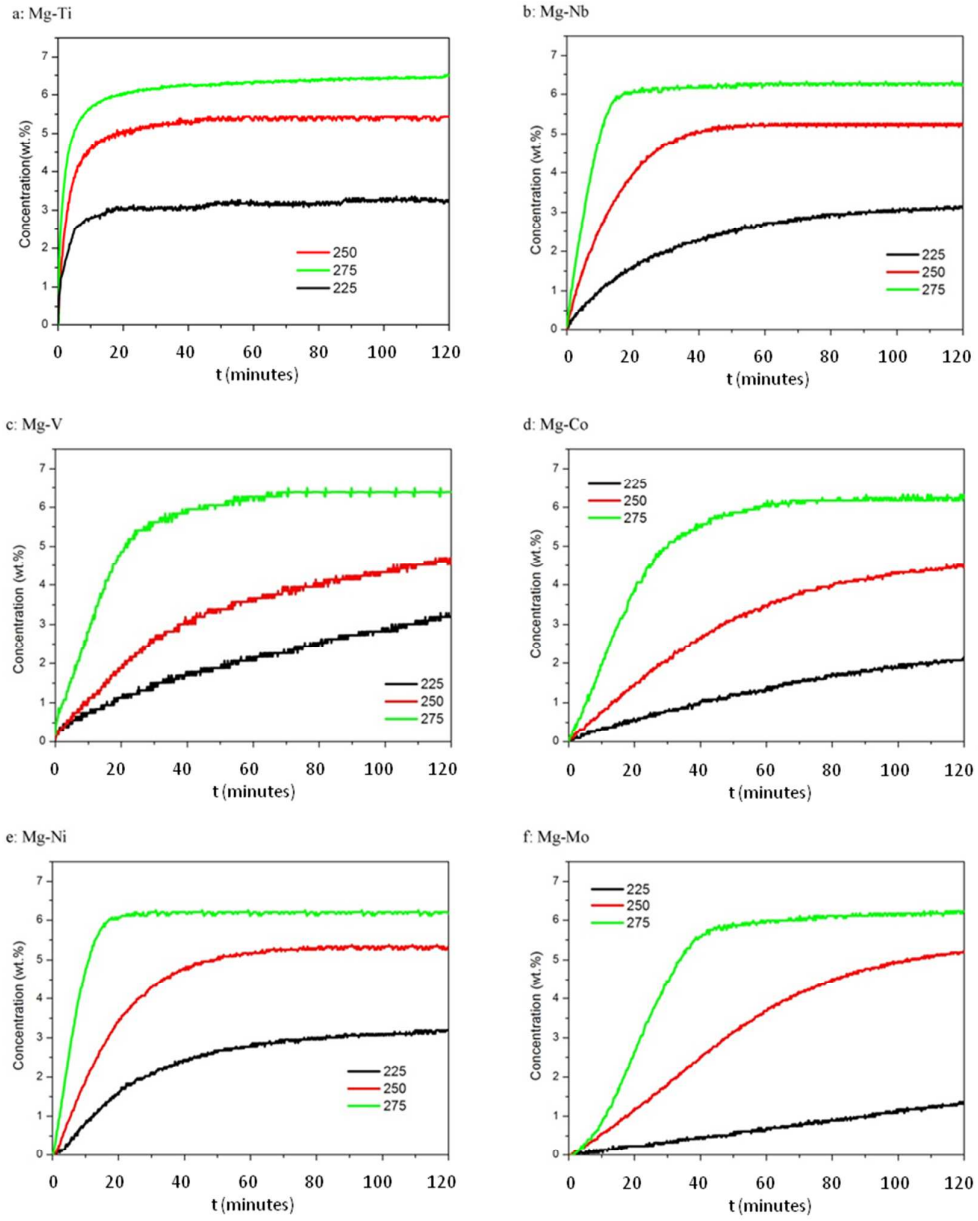

Fig. 7 Isothermal dehydrogenation curves of Mg-TM samples at 225, 250, and 275 °C.

a: Mg-Ti; b: Mg-Nb; c: Mg-V; d: Mg-Co; e: Mg-Ni; f: Mg-Mo.

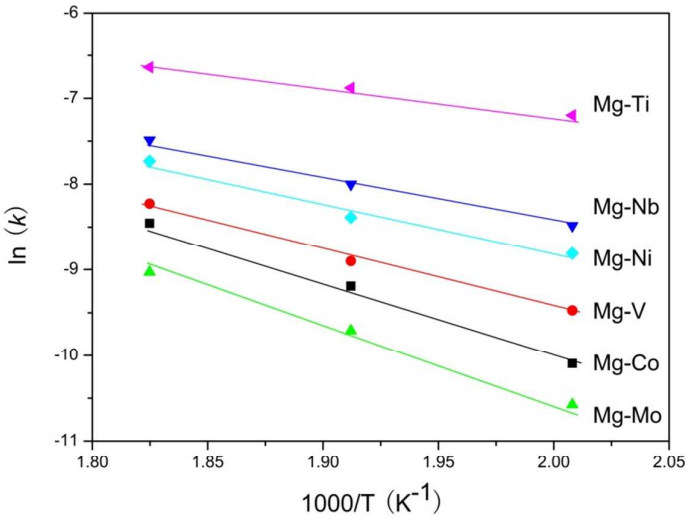

Fig. 8 Arrhenius plots of the absorption rate for the Mg-TMsamples

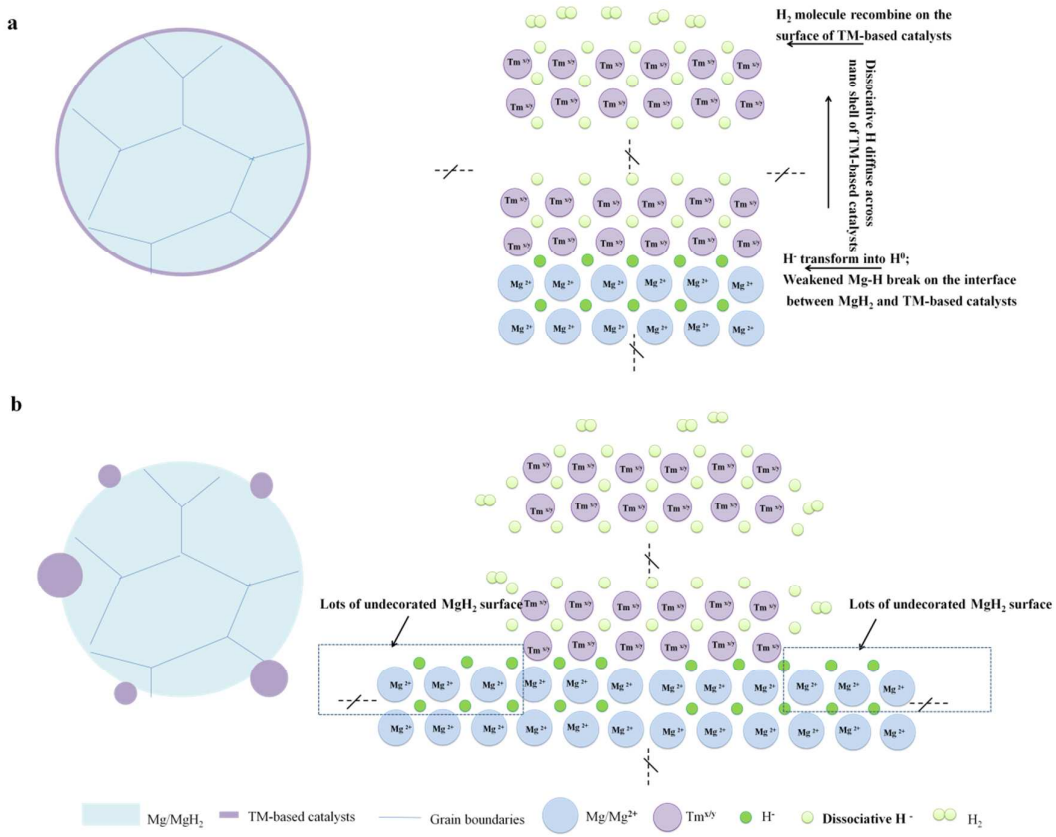

Fig. 9 The section schematic diagram of Mg-TM and ball-milled Mg-TM-based catalyst

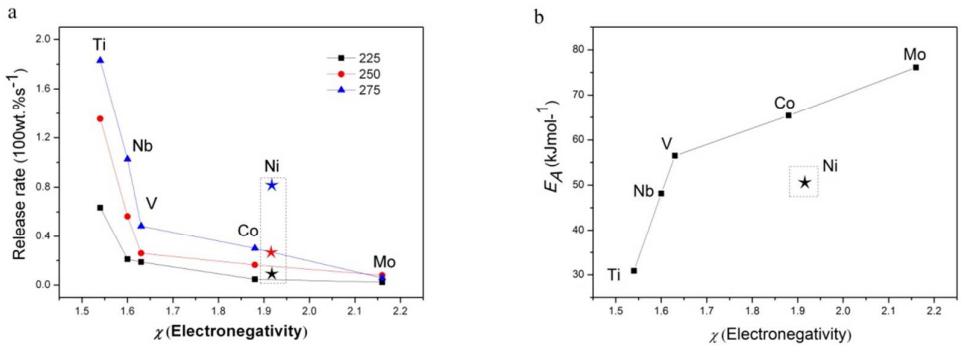

Fig. 10 a: Comparison in dehydrogenation average kinetics within 5 minutes of Mg-TM samples at 225, 250 and 275 °C; b: The plot of E_A vs χ of TM in Mg-TM systems.

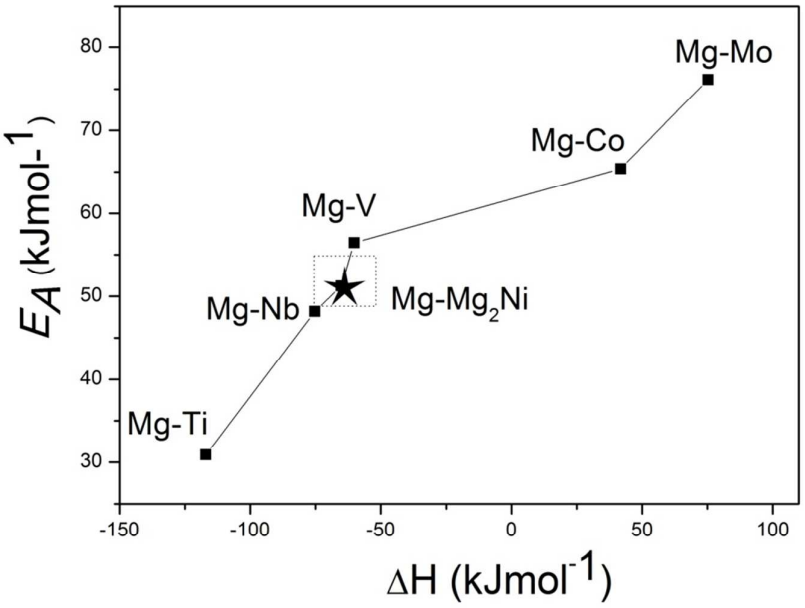

Fig. 11 The plot of E_A vs formation enthalpy of TMH_x in Mg-TM systems.

Table 1 The grain size determined from direct application of the Scherrer equation (without corrections for stress) to selected phases of Mg-TM samples under varying state.

Grain size (nm) / Phases	as prepared	hydrogenated after cycles		dehydrogenated after cycles	
Ti	15±3	TiH_2	17±3	TiH_2	14±2
Nb	9±2	Nb	11±3	Nb	11±3
V	20±2	V	16±2	V	15±3
Ni	19±2	Mg_2NiH_4	21±3	Mg_2Ni	16±3
Co	16±3	Co	17±3	Co	19±3
Mo	9±2	Mo	16±3	Mo	11±3

Table 2 EDS anlysis in different areas of as prepared BM-R sample.

	1	2	3	4	5	6
Mg	75.8	64.3	71.2	62.6	90.2	87.6
Ni	24.2	35.7	28.8	37.4	9.8	12.4

Table 3 Activation Energy for dehydrogenation and the electro-negativity of TM indifferent Systems.

systems	electro-negativity of TM (χ)	E_A (kJmol^{-1})
Mg-Ti	1.54	30.9
Mg-Nb	1.60	48.2
Mg-V	1.63	56.5
Mg-Ni	1.91	51.2
Mg-Co	1.88	65.4
Mg-Mo	2.16	76.1
Ball-milled Mg-$TiCl_3$	1.54	77.6